Modulation of immune cell reactivity with *cis*-binding Siglec agonists

Corleone S. Delaveris[a,b], Shannon H. Chiu[a,b], Nicholas M. Riley[a], and Carolyn R. Bertozzi[a,b,c,1]

[a]Department of Chemistry, Stanford University, Stanford, CA 94305; [b]Stanford ChEM-H, Stanford University, Stanford, CA 94305; and [c]HHMI, Stanford University, Stanford, CA 94305

Edited by Alanna Schepartz, Yale University, New Haven, CT, and approved December 3, 2020 (received for review June 22, 2020)

Inflammatory pathologies caused by phagocytes lead to numerous debilitating conditions, including chronic pain and blindness due to age-related macular degeneration. Many members of the sialic acid-binding immunoglobulin-like lectin (Siglec) family are immunoinhibitory receptors whose agonism is an attractive approach for antiinflammatory therapy. Here, we show that synthetic lipid-conjugated glycopolypeptides can insert into cell membranes and engage Siglec receptors in *cis*, leading to inhibitory signaling. Specifically, we construct a *cis*-binding agonist of Siglec-9 and show that it modulates mitogen-activated protein kinase (MAPK) signaling in reporter cell lines, immortalized macrophage and microglial cell lines, and primary human macrophages. Thus, these *cis*-binding agonists of Siglecs present a method for therapeutic suppression of immune cell reactivity.

glycocalyx | glycopolymer | Siglec | immunotherapy | inflammation

Sialic acid-binding immunoglobulin (IgG)-like lectins (Siglecs) are a family of immune checkpoint receptors that are on all classes of immune cells (1–5). Siglecs bind various sialoglycan ligands and deliver signals to the immune cells that report on whether the target is healthy or damaged, "self" or "nonself." Of the 14 human Siglecs, 9 contain cytosolic inhibitory signaling domains. Accordingly, engagement of these inhibitory Siglecs by sialoglycans suppresses the activity of the immune cell, leading to an antiinflammatory effect. In this regard, inhibitory Siglecs have functional parallels with the T cell checkpoint receptors CTLA-4 and PD-1 (6–9). As with these clinically established targets for cancer immune therapy, there has been a recent surge of interest in antagonizing Siglecs to potentiate immune cell reactivity toward cancer (10). Conversely, engagement of Siglecs with agonist antibodies can suppress immune cell reactivity in the context of antiinflammatory therapy. This approach has been explored to achieve B cell suppression in lupus patients by agonism of CD22 (Siglec-2) (11, 12), and to deplete eosinophils for treatment of eosinophilic gastroenteritis by agonism of Siglec-8 (13). Similarly, a CD24 fusion protein has been investigated clinically as a Siglec-10 agonist for both graft-versus-host disease and viral infection (14, 15).

Traditionally, Siglec ligands have been studied as functioning in *trans*, that is, on an adjacent cell (16–18), or as soluble clustering agents (9, 19). In contrast to these mechanisms of action, a growing body of work suggests that *cis* ligands for Siglecs (i.e., sialoglycans that reside on the same cell membrane) cluster these receptors and maintain a basal level of inhibitory signaling that increases the threshold for immune cell activation. Both Bassik and coworkers (20) and Wyss-Coray and coworkers (21) have linked the depletion of *cis* Siglec ligands with increased activity of macrophages and microglia, and other studies have shown that a metabolic blockade of sialic acid renders phagocytes more prone to activation (22).

Synthetic ligands are a promising class of Siglec agonists (17, 23, 24). Many examples rely on clustering architectures (e.g., sialopolymers, nanoparticles, liposomes) to induce their effect (19, 23–26). Indeed, we have previously used glycopolymers to study the effects of Siglec engagement in *trans* on natural killer (NK) cell activity (16). We and other researchers have employed glycopolymers (16, 23), glycan-remodeling enzymes (27, 28), chemical inhibitors of glycan biosynthesis (22), and mucin overexpression constructs (29, 30) to modulate the cell-surface levels of Siglec ligands. However, current approaches lack specificity for a given Siglec.

We hypothesized that Siglec-specific *cis*-binding sialoglycans displayed on immune cell surfaces could dampen immune cell activity with potential therapeutic applications. Here we test this notion with the synthesis of membrane-tethered *cis*-binding agonists of Siglec-9 (Fig. 1). Macrophages and microglia widely express Siglec-9 and are responsible for numerous pathologies including age-related inflammation (31), macular degeneration (32), neural inflammation (33), and chronic obstructive pulmonary disease (34). We designed and developed a lipid-linked glycopolypeptide scaffold bearing glycans that are selective Siglec-9 ligands (**pS9L-lipid**). We show that **pS9L-lipid** inserts into macrophage membranes, binds Siglec-9 specifically and in *cis*, and induces Siglec-9 signaling to suppress macrophage activity. By contrast, a lipid-free soluble analog (**pS9L-sol**) binds Siglec-9 but does not agonize Siglec-9 or modulate macrophage activity. Membrane-tethered glycopolypeptides are thus a potential therapeutic modality for inhibiting phagocyte activity.

Results

Glycopolypeptides Were Synthesized by *N*-Carboxyanhydride Polymerization. We designed biomimetic *cis* ligands for Siglecs by taking inspiration from mucins, heavily glycosylated polypeptides

Significance

Cells are covered in a dense forest of sugars. The abundance of specific sugar structures can influence immune cell activation, in part through a class of sugar-binding immune receptors known as Siglecs. However, the effects of Siglecs engaged by *cis* ligands are poorly understood. Thus, to elucidate these interactions, in this work we developed biomimetic structures of native glycoproteins bearing selective Siglec ligands. We demonstrate that these structures bind Siglec receptors and stimulate Siglec signaling when used as membrane-tethered *cis* ligands but that soluble analogs lacking a membrane-tethering lipid do not. These results present *cis* ligands as a way to target Siglecs in inflammatory diseases.

Author contributions: C.S.D. and C.R.B. designed research; C.S.D., S.H.C., and N.M.R. performed research; C.S.D., N.M.R., and C.R.B. analyzed data; and C.S.D. and C.R.B. wrote the paper.

Competing interest statement: C.S.D. and C.R.B. are coinventors on a patent application related to this work (USPTO63046140). C.R.B. is a cofounder and scientific advisory board member of Lycia Therapeutics, Palleon Pharmaceuticals, Enable Bioscience, Redwood Biosciences (a subsidiary of Catalent), and InterVenn Biosciences, and a member of the board of directors of Eli Lilly & Company.

This article is a PNAS Direct Submission.

[1]To whom correspondence may be addressed. Email: bertozzi@stanford.edu.

This article contains supporting information online at https://www.pnas.org/lookup/suppl/doi:10.1073/pnas.2012408118/-/DCSupplemental.

Published January 11, 2021.

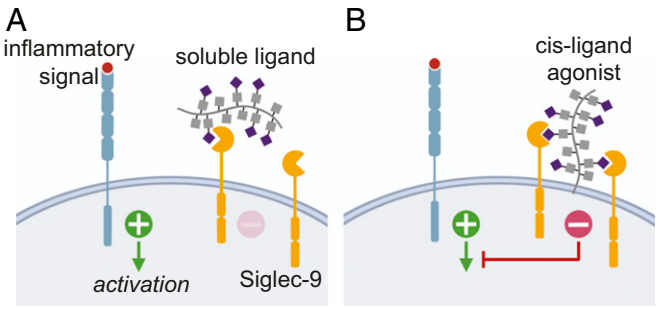

Fig. 1. Lipid-tethered glycopolypeptides cluster and agonize Siglecs in *cis* on effector cells. (*A*) Immune cells express activating receptors that stimulate inflammatory signaling. (*B*) Clustering of Siglec-9 by *cis*-binding agonists stimulates inhibitory signaling that quenches activation.

that are native Siglec ligands (9). To construct the glycopolypeptide backbone, we employed an *N*-carboxyanhydride (NCA) polymerization platform. We polymerized NCA monomers using lipid-tethered initiators to afford lipid-tethered polypeptides that spontaneously insert into cell membranes. In order to elaborate our glycopolypeptide scaffold, we combined the enzymatic methods from Chen and coworkers (35) that we have used previously (36) with the sialic acid analogs previously reported by Paulson and coworkers to bind specific Siglecs with high affinity and selectivity (26). High-affinity Siglec ligands achieved by derivatizing sialic acids at the C5 and/or C9 positions have been previously reported (26, 37–42). These ligands have monomeric dissociation constants in the low micromolar to single-digit nanomolar range (37). The Siglec ligands used in this work were those reported by Paulson and coworkers (26), and chosen due to their synthetic accessibility, although they had not previously been investigated for *cis*-ligand potential. We hypothesized that lipid-linked sialoglycopolypeptides incorporating these structures would insert into cell membranes and cluster neighboring Siglec receptors via *cis* binding.

Glycopolypeptide scaffolds were synthesized by polymerization of an equimolar mixture of alanine NCA **1** and *O*-β-peracetyllactose serine NCA **2** (Scheme 1*A*). Polymerizations were initiated either with an Ni(0) complex to afford a soluble glycopolypeptide or by precomplexing Ni(0) with a lipid-conjugated *N*-allylcarboxy leucine amide to form an activated Ni(II) initiator complex, **3**, as previously described (36, 43). The lipid-conjugated initiator affords a C-terminally conjugated lipid on the polypeptide. After polymerization, the carbohydrate was deprotected with hydrazine to afford the *O*-lactosyl glycopolypeptides **pLac-sol** or **pLac-lipid**, respectively.

We used a one-pot multienzyme system to α-2,6-sialylate common **pLac** precursors (Scheme 1*B*) with 5-*N*-acetylneuraminic acid (for **pSia**), 9-*N*-propargylcarboxy-5-*N*-acetylneuraminic acid (for **pS7L**), or *N*-propargylcarboxymannosamine **4** with sodium pyruvate and a neuraminic acid aldolase (for **pS9L**). After enzymatic elaboration, high-affinity Siglec ligands were synthesized from alkyne-bearing intermediates by Huisgen cycloaddition using either adamantylazide (for **pS7L**) or benzhydrylazide (for **pS9L**). This afforded glycopolypeptides bearing either a C-terminal lipid or soluble group, a free N terminus, and glycans bearing terminal high-affinity Siglec ligands. Finally, polypeptides were N-terminally labeled with commercially available biotin or Alexa Fluor *N*-hydroxysuccinimide esters (*SI Appendix*, *Materials and Methods*).

pS9L-Lipid Inserts into Cell Membranes and Binds Siglec-9 in *Cis*. We constructed a panel of N-terminally labeled sialylated glycopolypeptides from the common precursors **pLac-lipid** or **pLac-sol** (Scheme 1*B*). We tested the binding of the constructs to recombinant soluble Siglec-Fc fusion proteins (44) in vitro and on cell surfaces. In vitro, each glycopolypeptide bound specifically to its cognate Siglec receptor (Fig. 2 *A* and *B*) (*SI Appendix*, Fig. S1). For example, **pS9L-sol** bound to Siglec-9-Fc with high affinity but did not bind any other recombinant Siglec-Fc (Fig. 2*B*). We measured the kinetics of **pS9L-lipid** association in a similar manner, and from those observations calculated comparable apparent K_D values (~50 nM) for the **pS9L-sol** and **pS9L-lipid** constructs (Fig. 2*B* and *SI Appendix*, Fig. S1). We observed similar specificity when lipid-conjugated versions were inserted into cell membranes and the cells were stained with recombinant Siglec-9-Fc (Fig. 2 *C* and *D*). Glycan-dependent variation in the insertion of glycopolypeptides was consistent with what we have observed in previous glycocalyx engineering studies (*SI Appendix*, Fig. S2) (16). Previous studies using similar lipid-tethered glycopolypeptides have shown that polymers with these lipid tails will spontaneously insert into lipid bilayers and vesicles (36), and thus the lipid tails likely insert into the cell membrane during labeling, as has been observed with previous generations of glycopolymers (16, 45). Mutation of Siglec-9 R120A, a loss-of-sialic acid binding mutant (46), abrogated the effect observed in both the in vitro and flow experiments (Fig. 2*B*) (*SI Appendix*, Figs. S1 and S3), and staining with *Sambucus nigra* lectin showed no increase in binding for any structures (*SI Appendix*, Fig. S4).

To determine whether lipid-tethered glycopolypeptides associated with Siglecs in *cis*, we measured Förster resonance energy transfer (FRET) between the fluorophores of lipid-linked glycopolypeptides N-terminally labeled with an Alexa Fluor 555 donor fluorophore and anti-Siglec antibodies conjugated to an Alexa Fluor 647 acceptor (Fig. 3*A*). We excited the donor fluorophore with a 561-nm laser and detected fluorescence with both 605- and 685-nm-emission filters. We quantified FRET signal using a simplified version of FRET efficiency known as relative efficiency (E_{rel}), which is the ratio of acceptor fluorescence intensity to the sum of acceptor and donor fluorescence intensities.

We analyzed glycopolypeptide specificity using **pS9L-lipid** and **pS7L-lipid** displayed on Siglec-9–expressing cells (Fig. 3 *B* and *D*) and Siglec specificity using **pS9L-lipid** on Siglec-9– or Siglec-7–expressing cells (Fig. 3 *C* and *E*). We observed dramatic increases in relative FRET efficiency only when **pS9L-lipid** was paired with Siglec-9, but not in any of the mismatched cases (Fig. 3 *D* and *E*). Furthermore, we observed intense puncta when Siglec-9 and **pS9L-lipid** were present together on the cell surface. An alternate way to measure FRET efficiency is to compare the acceptor emission intensity of the FRET pair with an acceptor-only control. A significant increase in acceptor emission intensity was observed between the FRET pair and acceptor-only control on cells coated with **pS9L-lipid** expressing Siglec-9 but not with Siglec-7 (*SI Appendix*, Fig. S5). Together, these data show that **pS9L-lipid** is a *cis*-binding and selective ligand for Siglec-9.

***Cis*-Binding but Not Soluble pS9L Inhibits TLR4-Induced NF-κB Activity in Siglec-9–Expressing HEK Cells.** Previous work has shown that Siglec-3, which has a similar signaling domain to Siglec-7 and -9, can dampen the response of hTLR4 stimulation by bacterial lipopolysaccharide (LPS) (47). Therefore, we tested the effects of *cis*-ligand engagement of Siglec-7 and -9 by their respective glycopolypeptide ligands on this innate immune response. We developed a reporter system for Siglec activity based on the commercially available HEKBlue hTLR4 reporter assay (InvivoGen; hkb-htlr4). In this assay, LPS-induced hTLR4 signaling initiates nuclear factor kappa B (NF-κB)-mediated transcription of secreted embryonic alkaline phosphatase (SEAP), which is released into the media and quantitated with a colorimetric assay. We transfected HEKBlue cells with expression plasmids encoding Siglec variants (Fig. 4*A*) (48). In order to validate that

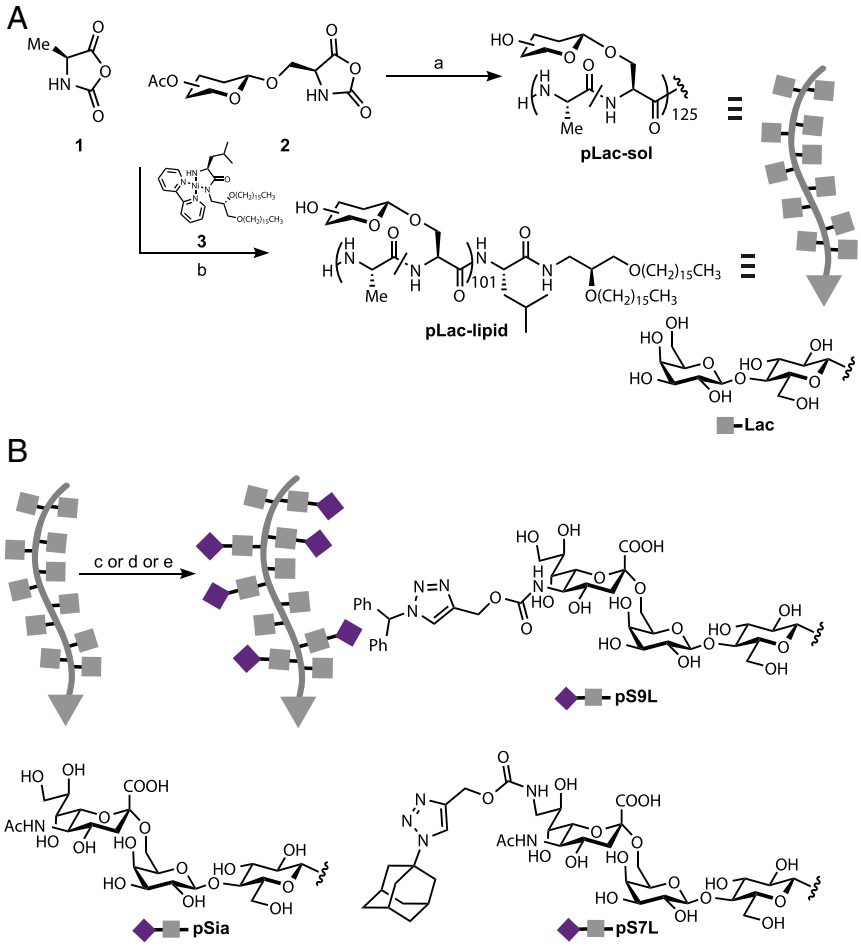

Scheme 1. (*A*) Synthesis of **pLac-sol** and **pLac-lipid** glycopolypeptide scaffolds. (*A*, *a*) THF, Ni(1,1′-bipyridine)(1,5-cyclooctadiene), 22 °C, glovebox; hydrazine monohydrate, MeOH/THF/H_2O, 24 h at 22 °C; 65% over two steps. Soluble polymers have a decarboxylated Ala or Ser residue at the C terminus, whichever initiated polymerization for a particular polymer; for a description of the mechanism by which the decarboxylated C-terminal amino acid is generated, see the work by Deming et al. (76). (*A*, *b*) THF, **3**, 6 h at 22 °C, glovebox; hydrazine monohydrate, MeOH/THF/H_2O, 24 h at 22 °C; 85% over two steps. (*B*) Chemoenzymatic elaboration of lactosyl glycopolypeptide scaffold. Syntheses are representative of both **-lipid** and **-sol** constructs. (*B*, *c*) For **pSia**: Neu5Ac, CTP, Pd26ST, NmCSS, 20 mM $MgCl_2$ in 200 mM Tris (pH 8.5), 48 h; 94% recovery with 45% conversion for **pSia-lipid**, 95% mass recovery with 50% conversion for **pSia-sol**. (*B*, *d*) For **pS9L**: 2-*N*-propargylcarboxymannosamine, CTP, sodium pyruvate, Pd26ST, NmCSS, NanA, 20 mM $MgCl_2$ in 200 mM Tris (pH 8.5), 48 h; benzhydrylazide, $CuSO_4$, BTTAA, tBuOH/H_2O, 12 h at 22 °C; 85% mass recovery and 22% conversion for **pS9L-lipid**, 85% mass recovery and 39% conversion for **pS9L-sol** over two steps. (*B*, *e*) For **pS7L**: 5-*N*-acetyl-9-propargylcarbamyl-9-deoxyneuraminic acid, CTP, Pd26ST, NmCSS, 20 mM $MgCl_2$ in 200 mM Tris (pH 8.5), 48 h; adamantylazide, $CuSO_4$, BTTAA, tBuOH/H_2O, 12 h at 22 °C; 30% mass recovery and 27% conversion for **pS7L-lipid**, 45% mass recovery and 25% conversion for **pS7L-sol** over two steps.

Siglec-9 signaling can suppress hTLR4 signaling in these cells, we agonized Siglec-9 transfectants with immobilized antibody (49). We plated Siglec-9 transfectants on plates coated with an agonistic anti–Siglec-9 antibody (clone 191240) (50) followed by hTLR4 stimulation with LPS. As shown in Fig. 4*B*, we observed a significant reduction in SEAP activity compared with cells grown on untreated or isotype antibody-coated plates, indicating that Siglec-9 signaling modulates NF-κB activity in this model system.

Next, Siglec-9–expressing HEKBlue cells were incubated with **pS9L-lipid** or **pS9L-sol** (1 μM) and then washed before stimulation with LPS. We observed reduced NF-κB activity with *cis*-binding **pS9L-lipid** but not with the soluble ligand **pS9L-sol** (Fig. 4*C*) or with other lipid-tethered glycopolypeptides (*SI Appendix*, Fig. S7). To test the Siglec specificity of **pS9L-lipid**, HEKBlue cells were transfected with a Siglec-9, Siglec-7, or mock vector and coated with **pS9L-lipid** (1 μM) before stimulation with LPS. We observed that only **pS9L-lipid** inhibited NF-κB activity compared with vehicle-treated cells when the cells expressed Siglec-9 (Fig. 4*D*). Cells that expressed mutant Siglec-9 lacking glycan-binding activity (R120A) or a double mutant (Y433/456F) that prevents tyrosine phosphorylation, and thus immune suppressive signaling (51), displayed the same response to LPS stimulation when treated with **pS9L-lipid** or vehicle (Fig. 4*E*) (*SI Appendix*, Fig. S8). These data demonstrate that *cis* engagement of Siglec-9 with glycopolypeptides suppresses hTLR4 signaling and downstream inflammatory pathways.

***Cis*-Binding but Not Soluble pS9L Inhibits MAPK Signaling in Macrophages.** Macrophages are drivers of disease in many inflammatory conditions and typically express Siglec-9 (52, 53). THP-1 cells are an immortalized monocyte line that is widely used to study macrophage biology (54–56). Previous work has shown that either chemical (22) or genetic (20, 21) inhibition of sialoside biosynthesis, leading to a hyposialylated phenotype, can potentiate phagocytic activity of macrophages and other phagocytes. Although not studied in detail, these observations may result from *cis* engagement of and inhibitory signaling by resident Siglecs. To avoid confounding effects of endogenous *cis*-ligand activity in our studies, we generated a constitutively hyposialylated THP-1 cell line by CRISPR knockout (KO) of the

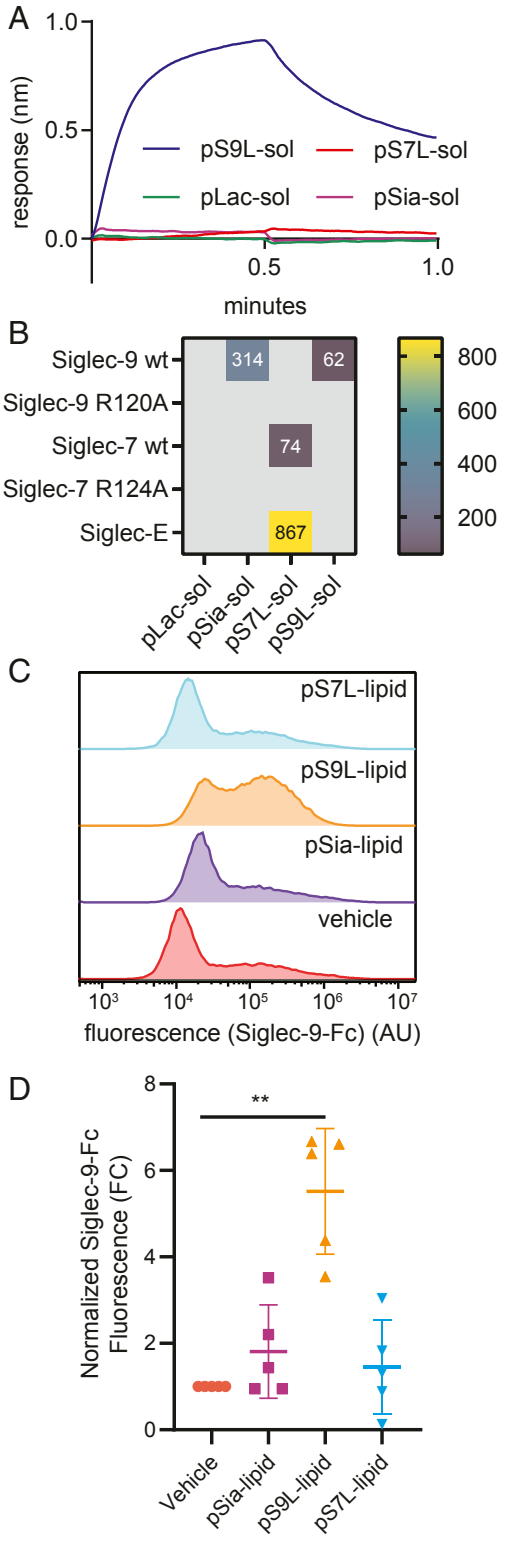

Fig. 2. Engineered glycopolypeptides bind Siglec-9 with high affinity. (*A* and *B*) Soluble glycopolypeptides bearing an N-terminal biotin were bound to streptavidin-coated tips. Association–dissociation curves were measured by dipping the tips into a solution of recombinant Siglec-Fc fusion protein followed by buffer only. Data are representative of two independent experiments. (*A*) Representative association then dissociation curves for the binding of Siglec-9-Fc fusion proteins to glycopolypeptides. (*B*) Composite data from all experiments. Gray cells indicate that an association–dissociation curve could not be fit due to undetectable specific binding. Apparent K_D values (nM) are shown in the corresponding cells. (*C* and *D*) Desialylated THP-1 monocytes were coated with lipid-tethered glycopolypeptides and stained with Siglec-9-Fc precomplexed with an anti-human Fc Alexa Fluor 647-conjugated secondary antibody. (*C*) Representative histograms from a single experiment. (*D*) Fold change from vehicle fluorescence (mean fluorescence intensity) was determined for each experimental replicate. Error bars are presented as SD. Statistics were determined by a paired mixed-effects model, $^{**}P < 0.01$. AU, arbitrary units; FC, fold change; WT, wild type.

gene encoding CMP-sialic acid synthetase (*CMAS*), a critical enzyme for sialoside biosynthesis (*SI Appendix*, Fig. S9) (21). These THP-1 monocytes were differentiated into Siglec-9$^+$ macrophages using phorbol-12-myristate-13-acetate (PMA) (56) and used to interrogate the effects of Siglec engagement on inflammatory activity. To assess the effects of *cis*-engaging Siglec ligands, macrophages were treated with glycopolypeptide, washed, and then stimulated with LPS. We analyzed early signaling cascades using quantitative phosphoproteomics and complemented this technique with cytokine quantitation at a later time point (Fig. 5*A*).

Secretion of proinflammatory cytokines was measured using a multiplexed cytometric bead assay for six human cytokines. Macrophages were pretreated with glycopolypeptide (500 nM) followed either by vehicle treatment or LPS stimulation for 18 h. Samples of the media were assayed for cytokine content. We observed marked decreases in interleukin-1β (IL-1β), IL-8, and tumor necrosis factor α (TNFα) in samples pretreated with *cis*-binding **pS9L-lipid** but not the soluble analog **pS9L-sol** (Fig. 5*B*) (*SI Appendix*, Fig. S10). IL-10 and IL-12p70 were below the limit of detection for this assay (<20 pg/mL).

Using a similar procedure, changes in the phosphoproteome were analyzed from lysates directly after pretreatment with glycopolypeptide or after subsequent LPS stimulation for 5 min (Fig. 5 *C*–*E*) (*SI Appendix*, Figs. S11–S13). Minimal changes were observed in resting macrophages treated with lipid-conjugated or soluble glycopolypeptides. However, dramatic differences in phosphorylation were observed between LPS-stimulated cells pretreated with *cis*-binding **pS9L-lipid** and those pretreated with **pS9L-sol** or **pLac-lipid**. Notably, phosphorylation correlating with decreased activity of mitogen-activated protein kinase (MAPK) signaling was observed in cells pretreated with *cis*-binding **pS9L-lipid** (*SI Appendix*, Fig. S12). We also found differential phosphorylation of SH2 domain-containing proteins (e.g., SHIP2 and PTPN7) (*SI Appendix*, Fig. S13). We validated downstream MAPK signaling by Western blot analysis of total nuclear factor kappa B inhibitor alpha (IκBα) and phospho-IκBα (Fig. 5*F*) (57). Macrophages pretreated with **pS9L-lipid** had both more total IκBα and less phosphorylation of IκBα at sites (S32/36) that signal degradation, compared with cells treated with **pS9L-sol**. We were unable to observe differential phosphorylation of phosphotyrosines on Siglec-9 at any time points assayed (*SI Appendix*, Fig. S15). Collectively, these data suggest that the *cis* ligand **pS9L-lipid** inhibits proinflammatory pathways by modulating MAPK signaling through the activation of specific phosphatases.

***Cis* Ligands for Siglec-9 and Siglec-E Inhibit Phagocytosis by Macrophages and Microglia.** Engagement of Siglec receptors has been shown to inhibit phagocytosis (21, 52, 58). We hypothesized that **pS9L-lipid** could inhibit phagocytosis via *cis* engagement and agonism of Siglec-9. To study this, macrophage phagocytosis of low-pH turn-on fluorescent (pHrodo red) beads was monitored by fluorescence microscopy (Fig. 6 *A* and *B*). Phagocytosis was quantified as the area of fluorescence above a background threshold observed over five images per well, with three wells per sample.

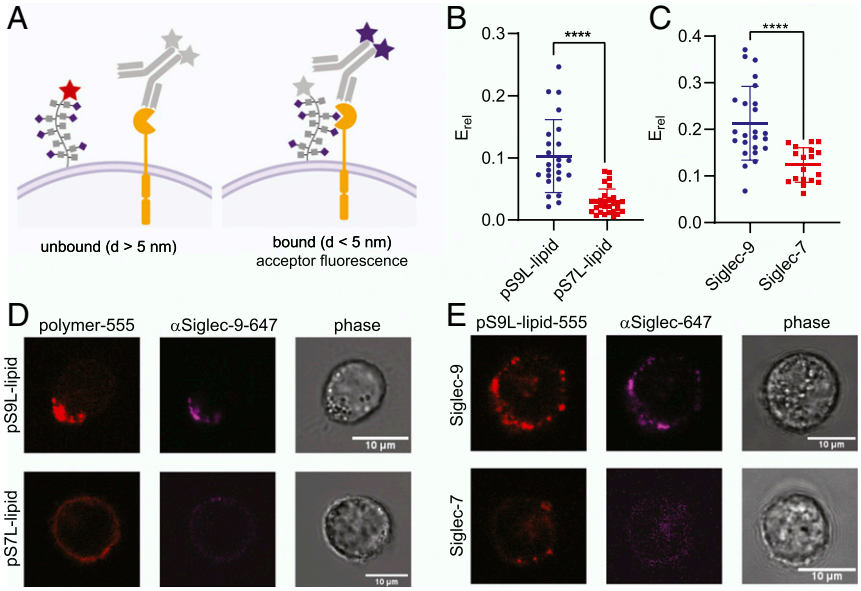

Fig. 3. **pS9L-lipid** associates in *cis* with Siglec-9 but not Siglec-7. (*A*) A FRET experiment to assess association of **pS9L-lipid** or **pS7L-lipid** with Siglec-9 or Siglec-7 in *cis*. Lipid-conjugated glycopolypeptide (**pS9L-lipid** or **pS7L-lipid**) was functionalized at the N terminus with Alexa Fluor 555 and loaded onto JURKATs stably expressing either Siglec-9 or Siglec-7. Anti-Siglec antibodies bearing Alexa Fluor 647 were bound to Siglec and FRET signal was quantified by fluorescence microscopy. (*B* and *D*) Relative FRET efficiency was calculated when **pS9L-lipid** or **pS7L-lipid** was loaded onto Siglec-9–expressing cells. Statistical analysis by one-way *t* test, ****$P < 0.0001$, Glass's $\Delta = 6.70$. (*C* and *E*) Relative FRET efficiency was calculated when **pS9L-lipid** was loaded onto Siglec-9– or Siglec-7–expressing cells. Statistical analysis by one-way *t* test, ****$P < 0.0001$, Glass's $\Delta = 2.42$. All data are representative of at least two independent experiments. Data points in *C* and *E* represent individual cells from a single experiment. Error bars are presented as SD.

Initially, we examined how **pS9L-lipid** affected early kinetics of phagocytosis. In brief, initial rates of phagocytosis were determined at multiple effector to target (E:T) ratios using wild-type THP-1 macrophages pretreated with **pS9L-lipid**, **pS9L-sol**, **pLac-lipid**, or vehicle only (Fig. 6*C*). Macrophages were incubated with glycopolypeptides for 3 h and then washed prior to the addition of various amounts of pHrodo-labeled beads. In the case of **pS9L-lipid**, we observed a dramatic reduction both in the rate of internalization at any given E:T ratio as well as the apparent maximum velocity of phagocytosis, whereas control glycopolypeptides yielded comparable results to vehicle-treated cells. Additionally, treatment with **pS9L-lipid** did not alter cell viability at least to 24 h (*SI Appendix*, Fig. S16). To determine whether the effect observed was mediated by Siglec-9 agonism, we generated a THP-1 CRISPR knockout of Siglec-9 (*SI Appendix*, Fig. S17) (21). While phagocytosis by hyposialylated CMAS KO THP-1 macrophages was potently inhibited by **pS9L-lipid** (Fig. 6*D*), KO of Siglec-9 completely abrogated the effect of **pS9L-lipid** on phagocytosis (Fig. 6*E*).

We next tested a small panel of glycoforms based on the same lipid-conjugated glycopolypeptide scaffold as **pS9L-lipid** (Fig. 6*F*). We observed that only **pS9L-lipid** significantly inhibited phagocytosis and this effect was dose-dependent (*SI Appendix*, Fig. S18). The Siglec-7–binding **pS7L-lipid** showed a trend toward phagocytosis inhibition but it was not statistically significant [THP-1 macrophages express Siglec-7 at low levels (56)]. We also assayed an analogous panel of soluble glycopolypeptides but observed no effect on phagocytosis (*SI Appendix*, Fig. S19). **pS9L-lipid** also inhibited phagocytosis of zymosan fungal particles (*SI Appendix*, Fig. S20).

The Siglec-7 ligand (**S7L**) identified by Paulson and coworkers was also a high-affinity ligand Siglec-E (26), the murine ortholog of human Siglec-7/9 (3). Thus, we hypothesized that **pS7L-lipid** may inhibit phagocytosis by Siglec-E–expressing cells. Indeed, we observed an inhibitory trend in murine microglia pretreated with **pS7L-lipid** (Fig. 6*G*) that was abrogated by CRISPR KO of Siglec-E (Fig. 6*H*). A stronger and statistically significant effect was observed compared with **pS9L-lipid**, which has negligible affinity for Siglec-E (*SI Appendix*, Fig. S22) (26).

To explore the translational relevance of our findings, we performed a similar assay with primary human macrophages. We isolated monocytes from healthy donor peripheral blood mononuclear cells (PBMCs) and differentiated them into resting (M0), M1, or M2 macrophages, and validated macrophage phenotype by flow cytometry (*SI Appendix*, Fig. S23) (59). The phagocytic activity of M0 and M1, but not M2, macrophages from five of six donors was inhibited by pretreatment with **pS9L-lipid** but not control polymers **pS9L-sol** or **pLac-lipid** (Fig. 7 *A*–*C*) (*SI Appendix*, Fig. S24). Following up on the single nonresponsive donor, we found that macrophages from this donor had dramatically lower levels of Siglec-9 expression (Fig. 7*D*). Thus, **pS9L-lipid** inhibits the phagocytic activity of both immortalized and primary macrophages via Siglec-9.

Discussion

We have demonstrated that Siglec-9 can be targeted by membrane-tethered *cis*-binding agonists to inhibit inflammatory signaling. The data presented here show that **pS9L-lipid** binds Siglec-9 in *cis* on the cell surface and induces immunosuppressive signaling both in immortalized and primary macrophages. This inhibition was dependent on functional Siglec-9 expression and signaling capability. The effect of **pS9L-lipid** on phagocytosis appeared to be entirely Siglec-9–dependent, as CRISPR KO of Siglec-9 in THP-1 macrophages completely abrogated activity. Furthermore, the suppressive effects of **pS9L-lipid** treatment on primary macrophages was stratified by Siglec-9 expression. Additionally, the concept of this work is supported by the recent preprint from Hong and coworkers, which details an enzymatic engineering approach to assemble high-affinity Siglec-7 ligands in situ on NK cells (60).

Based on phosphoproteomics analysis, the pathway most heavily affected by **pS9L-lipid**–Siglec-9 engagement was that of MAPK signaling (*SI Appendix*, Fig. S25). The effect was likely mediated by SH2-containing phosphatases in the PTN family,

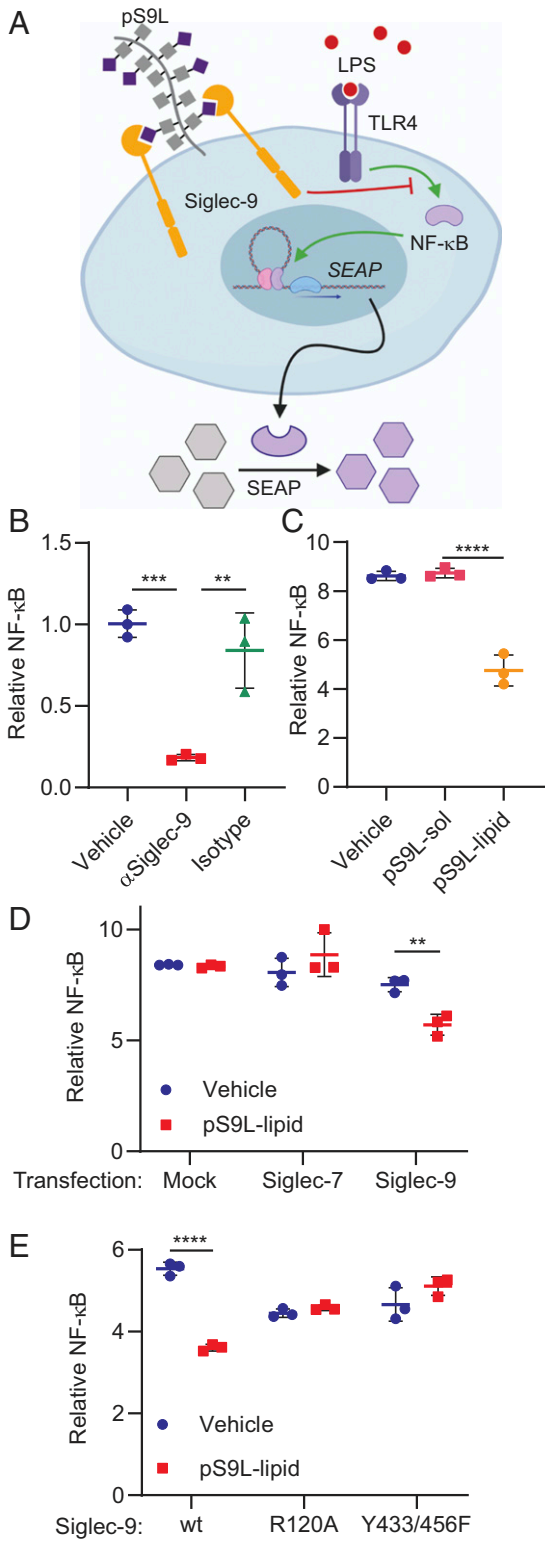

Fig. 4. **pS9L-lipid** agonizes Siglec-9 to inhibit TLR4 signaling in an NF-κB transcription reporter assay. (*A*) HEKBlue cells express both an NF-κB–dependent SEAP and the TLR4 signaling complex. Upon stimulation with LPS, SEAP in the supernatant can be quantified using a colorimetric assay as a proxy for NF-κB activity. For these assays, HEKBlue cells were also transfected with pCMV-Siglec expression vectors. (*B*) Siglec-9–expressing HEKBlue cells were grown on plates coated with antibody (anti–Siglec-9 clone 191240, isotype, or vehicle) and relative NF-κB transcription in response to LPS (10 ng/mL) was measured. (*C*) Siglec-9–expressing HEKBlue cells were pretreated with **pS9L-sol** (1 μM), **pS9L-lipid** (1 μM), or vehicle and washed prior to LPS stimulation (10 ng/mL). (*D*) HEKBlue cells were transfected with Siglec-9, Siglec-7, or a mock expression vector and coated with **pS9L-lipid** (1 μM) or vehicle and washed followed by LPS stimulation (10 ng/mL). (*E*) HEKBlue cells were transfected with a wild-type, R120A, or Y433/456F Siglec-9 expression vector and coated with **pS9L-lipid** (1 μM) or vehicle and washed followed by LPS stimulation (10 ng/mL). Statistics were determined by one-way (*B* and *C*) or two-way (*D* and *E*) ANOVA, $^{**}P < 0.01$, $^{***}P < 0.001$, $^{****}P < 0.0001$. Error bars are presented as SD. All data are representative of at least three independent experiments.

which includes the canonical Siglec-9 adaptor molecules SHP1 and SHP2. The effect of Y433/456F mutations in the HEKBlue reporter assay supports this hypothesis. Analysis of the differentially regulated phosphopeptides showed many downstream targets congruent with the activity of PTN phosphatases, the differential regulation of numerous SH2-containing proteins, and differential phosphorylation of specific PTN family members, such as PTPN7. The low abundance of phosphotyrosine relative to phosphoserine or -threonine leads to poor detection of phosphotyrosine residues using traditional phosphoproteomics enrichments (61), which may explain why differences in Siglec-9 phosphorylation and SHP1/2 signaling were not detected.

While we were unable to directly observe differential Siglec-9 phosphorylation by Western blot or phosphoproteomics, it may be the case that increased phosphorylation of Siglec-9 is not necessary for immune suppressive signaling. As seen in Fig. 3 *D* and *E*, the introduction of **pS9L-lipid** to Siglec-9–expressing cells caused the formation of puncta, whereas **pS9L-lipid** was evenly distributed around the cell membrane in Siglec-7–expressing cells. We hypothesize that polymeric presentation of Siglec-9 ligands by **pS9L-lipid** induces clustering of Siglec-9 into the observed puncta. The formation of these puncta would lead to a high localized concentration of Siglec-9, increasing the local concentration of phospho-ITIM/ISIM binding sites for immunoinhibitory phosphatases such as SHP1. This high local concentration of substrates could then lead to increased SHP1 (or similar phosphatases) at the membrane. This mechanism would be analogous to the antiphagocytic action of SIRPα that Morrissey and Vale recently described, wherein accumulation of SIRPα in a local environment leads to inhibitory signaling (62).

We consistently observed a robust and potent inhibitory response from lipid-tethered *cis* ligands but not from soluble ligands of comparable glycosylation density and molecular mass. There are multiple mechanisms by which the membrane-tethered analogs could induce signaling while the soluble versions cannot, including endocytosis of the ligand or the increased local concentration of sialoglycan ligands as lipid-tethered polymers accumulate in the membrane. Notably, monoclonal antibodies can be capable of agonizing Siglecs in a soluble format. An important example is the Siglec-8 antibody that has been approved for the treatment of certain eosinophilic inflammatory conditions (13, 63). Similarly, a CD24 antibody Fc fusion protein is being investigated to regulate inflammation through Siglec-10 (14, 15). However, there are settings in which a synthetic agonist might be preferable to an antibody, particularly in tissue compartments where long-term stability toward biodegradation is important, such as the eye or brain (64–67). Furthermore, synthetic *cis* agonists could be structurally tuned in ways antibodies cannot. For example, certain lipid tails, which we have previously synthesized on similar glycopolypeptides (36), have been shown to recycle on cells (45), and thus may present a route to long-lasting glycocalyx engineering. A major future direction is studying the application of *cis*-binding membrane-tethered agonists of Siglecs in translational inflammatory models. Although this work focuses on Siglec-9 on macrophages, the same protein modulates the activity of dendritic cells, subsets of T cells, and neutrophils, all of which play roles in other pathologies. Therefore,

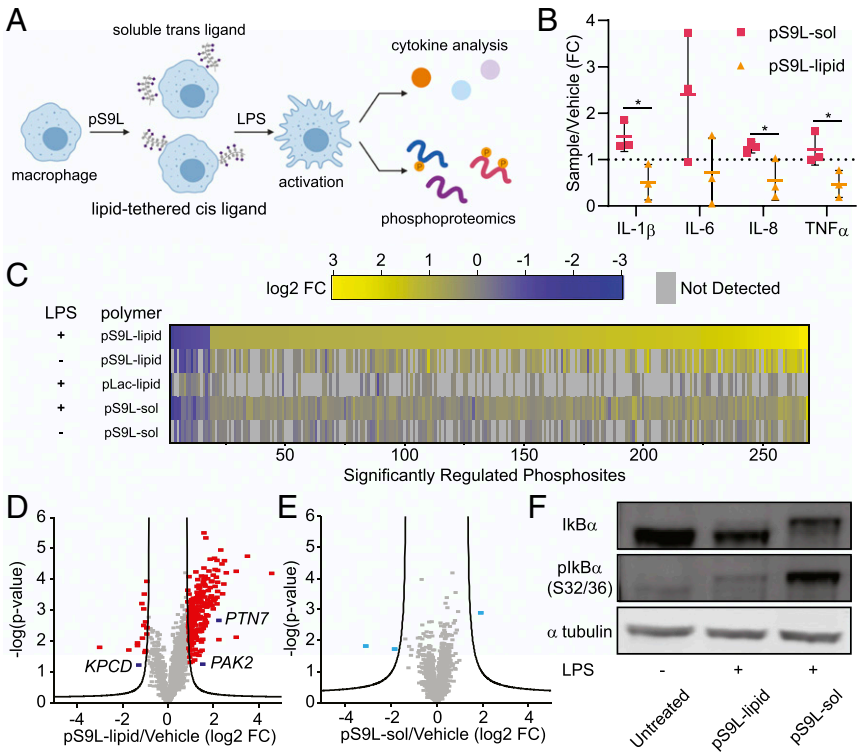

Fig. 5. Activation of macrophages is inhibited by *cis*-binding **pS9L-lipid** but not soluble ligand **pS9L-sol**. (*A*) Hyposialylated macrophages were pretreated with glycopolypeptide (500 nM) and subsequently washed and subjected to LPS stimulation (100 pg/mL). Activation was assayed by cytokine quantitation from the supernatant (*B*), quantitative phosphoproteomics (*C–E*), or Western blot (*F*). (*B*) Macrophages were pretreated with glycopolypeptide (500 nM) and then washed and stimulated with LPS (100 pg/mL) for 18 h. Aliquots of supernatant were analyzed by a multiplexed inflammatory cytokine assay. Data are presented as the fold change of averages of technical replicates from three independent experiments relative to vehicle-pretreated cells. Statistics were determined by multiple *t* tests, $*P < 0.05$. Error bars are presented as SD. (*C–E*) Macrophages were pretreated with glycopolypeptide (500 nM) and then washed and stimulated with LPS (100 pg/mL) for 5 min and lysed. Lysates were collected from three independent differentiations of macrophages. Lysates were normalized, enriched for phosphoproteins, labeled, and analyzed by quantitative phosphoproteomics. (*C*) A heatmap of fold change from macrophages pretreated with glycopolypeptides with or without LPS stimulation. (*D*) A volcano plot of significance vs. fold change over vehicle of macrophages pretreated with **pS9L-lipid** and stimulated with LPS. Significantly changed phosphopeptides identified are shown in red. Select unique hits are highlighted in dark blue. (*E*) As for *D*, but for **pS9L-sol**. (*F*) Macrophages were treated with glycopolypeptide (500 nM) and then washed and stimulated with LPS (100 pg/mL) for 1 h before lysis and analysis by Western blot for total IκBα and pIκBα (S32/36) levels. Lane 1 shows control macrophages that were treated with neither glycopolypeptide nor LPS.

the glycopolymers we report here may be broadly useful as modulators of both primary and secondary inflammatory reactions.

Materials and Methods

Detailed experimental procedures are available in *SI Appendix*. Characterization of synthetic materials is available in *SI Appendix* or previously published work.

Statistical Analysis. All statistical analyses were performed using GraphPad Prism 6.

Glycopolypeptide Synthesis. Glycopolypeptides were synthesized as previously described (36). In brief, *N*-carboxyanhydrides of alanine and *O*-lactosylserine were polymerized using precomplexed initiators to afford lipid-linked or soluble protected glycopolypeptides. The glycans were deacetylated using hydrazine and purified by dialysis. The polylactosyl scaffolds were then elaborated using a one-pot multienzyme system to afford various sialosides on the glycopolypeptide scaffold. Unnatural sialosides bearing alkyne handles were then reacted with azides to afford a polymeric presentation of previously described high-affinity Siglec ligands. The glycopolypeptides were used at various concentrations, as optimized for the specific cell type and application.

Human Cell Culture. Cell lines were cultured in either Dulbecco's modified Eagle's medium (DMEM) (HEKBlue hTLR4, BV2) or RPMI (JURKAT, THP-1) supplemented with 10% heat-inactivated fetal bovine serum (FBS). THP-1 culture media were further supplemented with 50 μM beta-mercaptoethanol. THP-1 monocytes were differentiated into macrophages by activating with PMA for 24 h followed by recovering in normal media for 24 h. PBMCs were isolated from buffy coats from whole blood or LRS chambers using Ficoll-Paque gradient centrifugation. Donors were deidentified before blood products were obtained. Monocytes were isolated by adherence onto tissue-culture plastic, as previously described (59, 68), and monocytes were differentiated into macrophages in RPMI-1640 containing 20% heat-inactivated FBS for 7 d with either no exogenous cytokines (M0), granulocyte-macrophage colony-stimulating factor (GM-CSF) (immature M1), GM-CSF for 5 d followed by LPS and interferon gamma in 10% heat-inactivated FBS for 2 d (activated M1), or M-CSF for 5 d followed by IL-4 and IL-13 in 10% heat-inactivated FBS for 2 d (M2).

In Vitro Protein Binding. Protein binding was recorded on an Octet Red96. For soluble glycopolypeptides, biotinylated ligands (200 nM) in phosphate-buffered saline (PBS) with bovine serum albumin (BSA) (0.1%) were loaded onto streptavidin-coated tips for 60 s (~0.4-nm response). Tips were then dipped into a serial dilution of Siglec-Fc and associated for 30 s and then dissociated in buffer for 30 s. For lipid-tethered glycopolypeptides, Siglec-9-Fc (200 nM) was loaded onto anti-hFc–coated tips for 60 s (~0.4-nm response). Tips were then dipped into a serial dilution of pS9L-lipid (2.5 μM to 25 nM) and associated for 60 s followed by dissociation for 120 s. In all experiments, tips were regenerated between washes in pH 1.5 glycine buffer.

Flow Cytometry. Cells were harvested and loaded with fluorophore-conjugated glycopolypeptide in serum-free media at a density of 10^7 cells per milliliter for 1 h with gentle agitation every 15 min. The cells were then

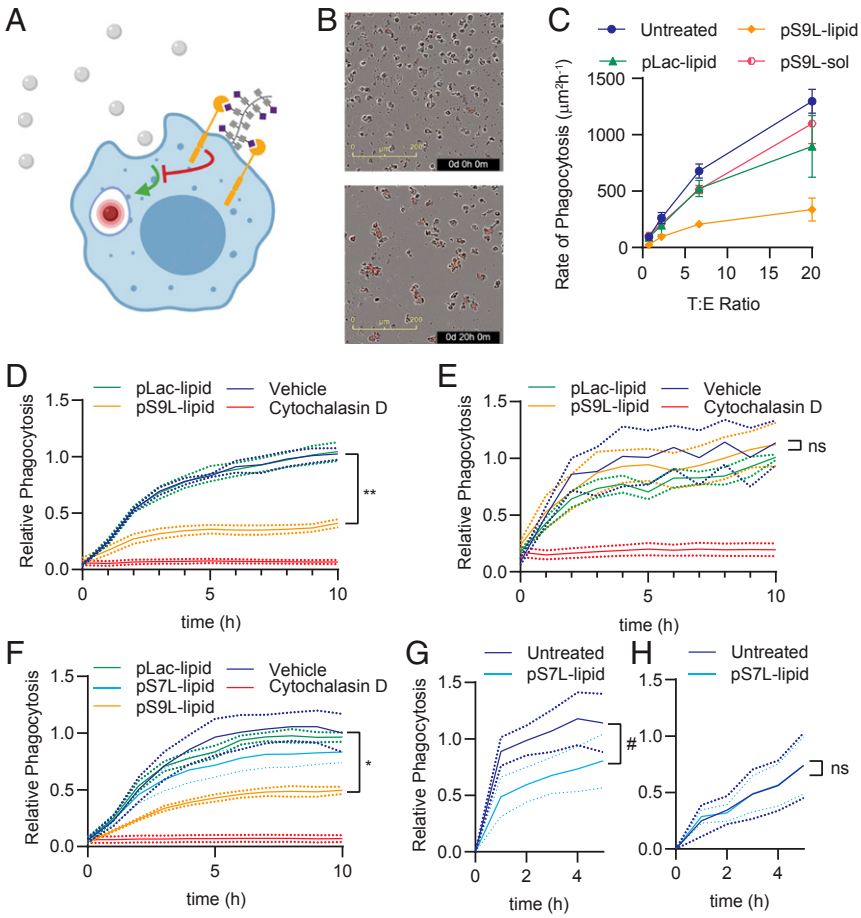

Fig. 6. **pS9L-lipid** inhibits macrophage phagocytosis in a Siglec-9–dependent manner. (*A*) Macrophage phagocytosis can be determined via fluorescence microscopy using beads that undergo fluorescence turn-on in acidic (i.e., late endosomal/lysosomal) compartments. (*B*) Representative images of merged phase and red fluorescence at 0 h (*Top*) and 15 h (*Bottom*). (*C*) THP-1 macrophages were pretreated with polymer (200 nM) for 3 h and washed, and a suspension of 1-μm pHrodo red-labeled beads was added at a given effector:target ratio. The initial rate of phagocytosis was determined by measuring the increase in red fluorescent area over the first hour. Data are representative of three independent experiments. (*D–F*) CMAS KO (*D*), Siglec-9 KO (*E*), or wild-type (*F*) THP-1 macrophages were pretreated with glycopolypeptide (200 nM) for 3 h, washed, and assayed for phagocytosis hourly for 10 h at an E:T ratio of 1:20 using 1-μm pHrodo red-labeled beads. (*G* and *H*) BV2 murine microglia with either a CRISPR safe-targeting guide (*G*) or a Siglec-E KO (*H*) were pretreated with neuraminidase (2 μM) and then loaded with the Siglec-E cross-reactive **pS7L-lipid** (500 nM) and washed before assaying phagocytosis as in *D–F*. For *D–H*, relative phagocytosis was determined for each individual experiment relative to the median end-point value of vehicle-treated cells in the same experiment. Statistical analysis by two-way ANOVA, $^{\#}P < 0.15$, $^{*}P < 0.05$, $^{**}P < 0.01$; ns, not significant. Error bars are presented as SEM. Data are representative of three independent experiments.

washed and stained with either a fluorophore-conjugated primary antibody or an unconjugated primary antibody with a fluorophore-conjugated anti-IgG secondary antibody at 4 °C and washed three times after staining. All flow analysis was done on unfixed cells.

Fluorescence Microscopy. FRET data were collected on a confocal microscope. JURKATs expressing Siglec-7 or -9 were suspended in serum-free RPMI at 10^7 cells per milliliter and labeled with Alexa Fluor 555-labeled glycopolypeptide (2 μM) for 1 h with gentle agitation every 15 min. Cells were washed and then labeled with Alexa Fluor 647-labeled anti–Siglec-7 or -9 antibody for 30 min at room temperature in complete media. The cells were washed with PBS and then plated onto live-cell imaging glass 8-well borosilicate no. 1.5 coverslips precoated with fibronectin. Cells were then imaged. For Siglec-9 immunocytochemistry, cells were fixed in 10% formalin, washed, and stained with Alexa Fluor 488-conjugated anti–Siglec-9 for 1 h on ice. Cells were then washed and imaged by 488-nm fluorescence on an Incucyte collecting five images per well with three wells per condition.

Cloning. An expression plasmid for PmNanA was constructed by InFusion cloning from a gBlock from IDT ligated into a PCR-linearized pET22b vector. CRISPR plasmids were constructed using guides optimized by the Bassik lab and cloned into the lentiCRISPR v2 plasmids using the GeCKO protocols (https://www.addgene.org/pooled-library/zhang-human-gecko-v2/) and purified by Miraprep (69). pCMV Siglec-9 mutants were generated using a Q5 mutagenesis kit (20, 69).

Protein Expression and Purification. PmNanA, Pd26ST, and NmCSS were expressed in BL21(DE3) *Escherichia coli* and isolated as previously described (35).

HEKBlue hTLR4 Reporter Assay. The HEKBlue hTLR4 assay was generally performed according to the manufacturer's instructions (InvivoGen). Cells were transfected 24 h before the assay using Lipofectamine LTX. For antibody-coated plate assays, plates were prepared by incubating 96-well plates with solution antibody (10 ng/mL) in PBS for 2 h at 37 °C and then washed three times with PBS before plating transfected cells. For glycopolypeptide assays, cells were harvested from the transfection plates, pelleted by centrifugation (300 relative centrifugal force [rcf], 5 min), and resuspended in a solution of glycopolypeptide (1 μM) in serum-free DMEM. Cells were mixed every 15 min for 1 h, at which point cells were washed with 1 mL complete media, counted, and plated.

Cytokine Bead Assay. CMAS KO THP-1 macrophages were cultured and labeled with glycopolypeptide (500 nM) for 3 h. At this point, the cells were washed and media with either vehicle or LPS (100 pg/mL) were added and cells were cultured for 18 h. Aliquots of media were then taken and

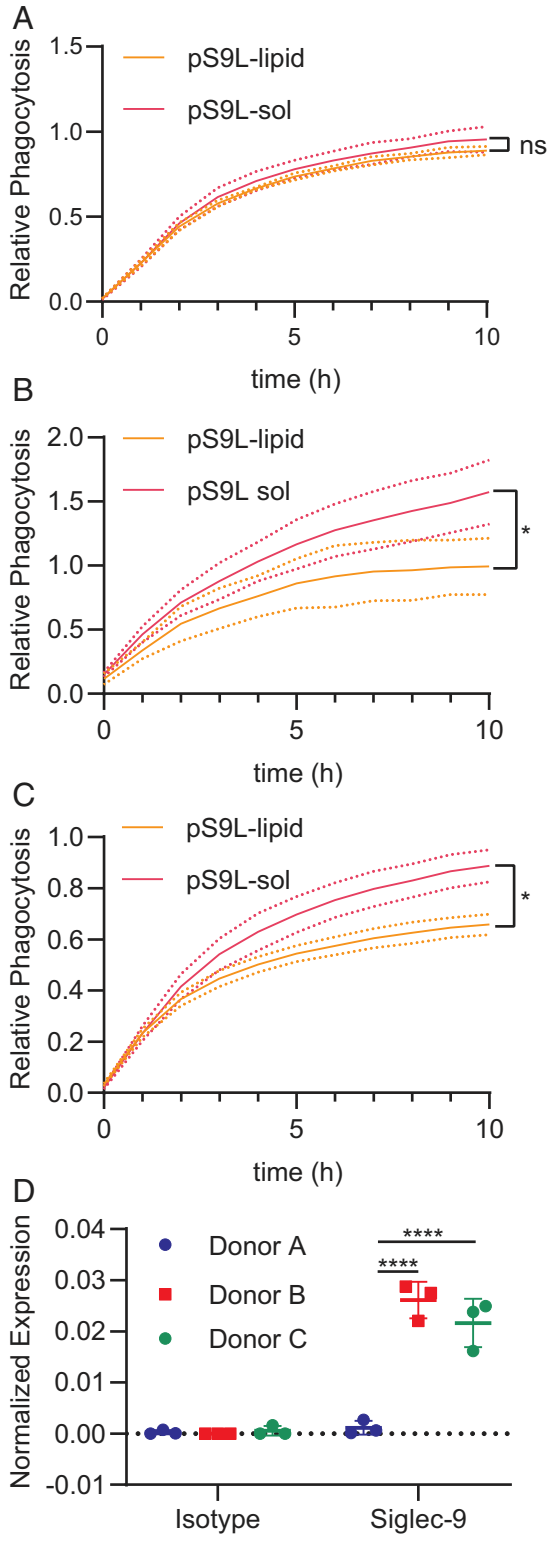

Fig. 7. Response to **pS9L-lipid** by monocyte-derived primary macrophages is stratified by Siglec-9 expression. Monocytes were isolated from PBMCs, differentiated into M1 macrophages by treatment with GM-CSF (50 ng/mL) for 6 d. (*A*–*C*) M1 macrophages differentiated from PBMCs isolated from three different donors were treated with glycopolypeptide (500 nM) for 3 h and washed before assaying phagocytosis of pHrodo-labeled beads at approximately a 1:20 E:T ratio. Statistical analysis by two-way ANOVA, $*P < 0.05$. Error bars are presented as SEM. (*D*) M1 macrophages were stained by microscopy with a fluorescently labeled anti–Siglec-9 antibody and fluorescence was quantified by microscopy. Donors A to C correspond to *A* to *C*. Normalized expression was determined by taking the ratio of the integrated fluorescence intensity per image by the confluency per image. Error bars are presented as SD. Statistical analysis by two-way ANOVA, $****P < 0.001$. Data are from three different donors.

flash-frozen at −80 °C. BD human inflammatory cytokine bead quantitation was then performed on thawed samples from three biological replicates in one batch according to the manufacturer's instructions.

Phosphoproteomics. CMAS KO THP-1 macrophages were cultured and labeled with glycopolypeptide (500 nM) in serum-free media for 3 h. At this point, the cells were washed and media with either vehicle or LPS (100 pg/mL) were added and cells were stimulated for 5 min. Cells were then lysed in cold RIPA buffer with benzonase and pelleted by centrifugation (18,000 rcf, 15 min, 4 °C), and supernatant protein concentrations were quantitated by Rapid Gold BCA.

Proteins were digested into tryptic peptides using an S-trap protocol (Protifi) (70) and were subsequently labeled with a 10-plex Tandem Mass Tag Set (Thermo Fisher Scientific). Phosphopeptides were enriched with Ti(IV)-IMAC beads (ReSyn Biosciences). Phosphopeptides and protein abundance samples were analyzed by liquid chromatography-tandem mass spectrometry (LC-MS/MS) using a Dionex UltiMate 3000 RPLC Nano System coupled to an Orbitrap Fusion (Thermo Fisher Scientific). Peptides were loaded onto a trap column (Acclaim PepMap 100 C18, 5-μm particles, 20-mm length; Thermo Fisher Scientific) and separated over a 25-cm EasySpray reversed-phase LC column (75-μm inner diameter packed with 2 μm particles of 100-Å PepMap C18; Thermo Fisher Scientific) using water with 0.2% formic acid (mobile phase A) and acetonitrile with 0.2% formic acid (mobile phase B). All methods totaled 180 min of acquisition time per analysis. Raw files were searched using the Andromeda algorithm and processed in MaxQuant (71, 72). Results were then processed in Perseus to calculate statistically significant changes in the phosphoproteome (73). Data have been deposited in the ProteomeXchange Consortium via the PRIDE partner repository with the dataset identifier PXD018774 (74).

Western Blot. CMAS KO THP-1 macrophages were cultured and labeled with glycopolypeptide (500 nM) in serum-free media for 3 h. At this point, the cells were washed and media with either vehicle or LPS (100 pg/mL) were added and cells were stimulated for 60 min. Cells were then lysed in cold RIPA buffer with benzonase and pelleted by centrifugation (18,000 rcf, 15 min, 4 °C), and supernatant protein concentrations were quantitated by BCA. Lysates were then run on sodium dodecyl sulfate-polyacrylamide gel electrophoresis using a 4 to 12% bisacrylamide gel at 200 V for 1 h in XT-MES. The gel was transferred to nitrocellulose using Trans-Blot Turbo transfer buffer at 25 V for 7 min. The blot was blocked with 5% BSA in Tris-buffered saline and stained with primary antibodies overnight at 4 °C, followed by incubation with an infrared dye-labeled secondary antibody at room temperature for 1 h. Blots were imaged by LI-COR.

Phagocytosis Assays. Phagocytes were treated with glycopolypeptide for 3 h in serum-free media. The cells were washed and coated with 100 μL serum-free media. Targets were then added as a suspension in 100 μL serum-free media. The plates were briefly centrifuged (300 rcf, 1 min) to settle the targets, and then phagocytosis was monitored by fluorescence microscopy on an Incucyte. Five images were collected per well for three wells per condition. For BV2 phagocytosis, BV2 cells were pretreated with recombinant, endotoxin-free *Vibrio cholerae* sialidase for 1 h at 2 μM prior to treating with glycopolypeptides.

Data Availability. Phosphoproteomics data have been deposited in the publicly accessible ProteomeXchange Consortium via the PRIDE partner repository with the dataset identifier PXD018774 (75). All other data discussed in this work are available in the main text or *SI Appendix*.

ACKNOWLEDGMENTS. We thank Simon Wisnovsky and Melissa A. Gray for their advice related to molecular biology analysis of Siglecs; Elizabeth R. Webster and Christopher J. Cambier for their advice on FRET microscopy; Payton Weidenbacher for assistance with Octet protein binding; and Stephen Lynch for his advice in acquiring and processing polymer NMR spectra. Plasmids containing Pd26ST and NmCSS were kind gifts from Xi Chen. The plasmid containing lentiCRISPRv2 was a gift from Feng Zhang (Addgene plasmid 52961; http://www.addgene.org/52961/; RRID:Addgene_52961). This work

was supported by National Cancer Institute Grant R01CA227942. C.S.D. was supported by an NSF Graduate Research Fellowship (DGE-114747) and a Stanford Interdisciplinary Graduate Fellowship affiliated with ChEM-H. S.H.C. was supported by a Stanford Bio-X Undergraduate Research Program Fellowship. N.M.R. was funded through an NIH Predoctoral to Postdoctoral Transition Award (Grant K00 CA21245403). Figure illustrations were created using BioRender.com.

1. T. K. Dam, C. F. Brewer, Lectins as pattern recognition molecules: The effects of epitope density in innate immunity. *Glycobiology* **20**, 270–279 (2010).
2. J. Y. Zhou, D. M. Oswald, K. D. Oliva, L. S. C. Kreisman, B. A. Cobb, The glycoscience of immunity. *Trends Immunol.* **39**, 523–535 (2018).
3. M. S. Macauley, P. R. Crocker, J. C. Paulson, Siglec-mediated regulation of immune cell function in disease. *Nat. Rev. Immunol.* **14**, 653–666 (2014).
4. P. R. Crocker, J. C. Paulson, A. Varki, Siglecs and their roles in the immune system. *Nat. Rev. Immunol.* **7**, 255–266 (2007).
5. B. S. Bochner, N. Zimmermann, Role of Siglecs and related glycan-binding proteins in immune responses and immunoregulation. *J. Allergy Clin. Immunol.* **135**, 598–608 (2015).
6. M. M. Gubin *et al*., Checkpoint blockade cancer immunotherapy targets tumour-specific mutant antigens. *Nature* **515**, 577–581 (2014).
7. H. Läubli *et al*., Engagement of myelomonocytic Siglecs by tumor-associated ligands modulates the innate immune response to cancer. *Proc. Natl. Acad. Sci. U.S.A.* **111**, 14211–14216 (2014).
8. C. Jandus *et al*., Interactions between Siglec-7/9 receptors and ligands influence NK cell-dependent tumor immunosurveillance. *J. Clin. Invest.* **124**, 1810–1820 (2014).
9. R. Beatson *et al*., The mucin MUC1 modulates the tumor immunological microenvironment through engagement of the lectin Siglec-9. *Nat. Immunol.* **17**, 1273–1281 (2016).
10. S. Duan, J. C. Paulson, Siglecs as immune cell checkpoints in disease. *Annu. Rev. Immunol.* **38**, 365–395 (2020).
11. A. Cesano, U. Gayko, CD22 as a target of passive immunotherapy. *Semin. Oncol.* **30**, 253–257 (2003).
12. T. Dörner *et al*., Initial clinical trial of epratuzumab (humanized anti-CD22 antibody) for immunotherapy of systemic lupus erythematosus. *Arthritis Res. Ther.* **8**, R74 (2006).
13. B. A. Youngblood *et al*., Siglec-8 antibody reduces eosinophils and mast cells in a transgenic mouse model of eosinophilic gastroenteritis. *JCI Insight* **4**, 126219 (2019).
14. R. R. Tian *et al*., CD24Fc protects against viral pneumonia in simian immunodeficiency virus-infected Chinese rhesus monkeys. *Cell. Mol. Immunol.* **17**, 887–888 (2020).
15. T. Toubai *et al*., Siglec-G-CD24 axis controls the severity of graft-versus-host disease in mice. *Blood* **123**, 3512–3523 (2014).
16. J. E. Hudak, S. M. Canham, C. R. Bertozzi, Glycocalyx engineering reveals a Siglec-based mechanism for NK cell immunoevasion. *Nat. Chem. Biol.* **10**, 69–75 (2014).
17. S. Spence *et al*., Targeting Siglecs with a sialic acid-decorated nanoparticle abrogates inflammation. *Sci. Transl. Med.* **7**, 303ra140 (2015).
18. A. Lizcano *et al*., Erythrocyte sialoglycoproteins engage Siglec-9 on neutrophils to suppress activation. *Blood* **129**, 3100–3110 (2017).
19. A. Shahraz *et al*., Anti-inflammatory activity of low molecular weight polysialic acid on human macrophages. *Sci. Rep.* **5**, 16800 (2015).
20. M. S. Haney *et al*., Identification of phagocytosis regulators using magnetic genome-wide CRISPR screens. *Nat. Genet.* **50**, 1716–1727 (2018).
21. J. V. Pluvinage *et al*., CD22 blockade restores homeostatic microglial phagocytosis in ageing brains. *Nature* **568**, 187–192 (2019).
22. C. Büll *et al*., Metabolic sialic acid blockade lowers the activation threshold of moDCs for TLR stimulation. *Immunol. Cell Biol.* **95**, 408–415 (2017).
23. A. H. Courtney, E. B. Puffer, J. K. Pontrello, Z.-Q. Yang, L. L. Kiessling, Sialylated multivalent antigens engage CD22 in *trans* and inhibit B cell activation. *Proc. Natl. Acad. Sci. U.S.A.* **106**, 2500–2505 (2009).
24. M. Perdicchio *et al*., Sialic acid-modified antigens impose tolerance via inhibition of T-cell proliferation and de novo induction of regulatory T cells. *Proc. Natl. Acad. Sci. U.S.A.* **113**, 3329–3334 (2016).
25. C. M. Nycholat *et al*., A sulfonamide sialoside analogue for targeting Siglec-8 and -F on immune cells. *J. Am. Chem. Soc.* **141**, 14032–14037 (2019).
26. C. D. Rillahan, E. Schwartz, R. McBride, V. V. Fokin, J. C. Paulson, Click and pick: Identification of sialoside analogues for Siglec-based cell targeting. *Angew. Chem. Int. Ed. Engl.* **51**, 11014–11018 (2012).
27. S. A. Malaker *et al*., The mucin-selective protease StcE enables molecular and functional analysis of human cancer-associated mucins. *Proc. Natl. Acad. Sci. U.S.A.* **116**, 7278–7287 (2019).
28. H. Xiao, E. C. Woods, P. Vukojicic, C. R. Bertozzi, Precision glycocalyx editing as a strategy for cancer immunotherapy. *Proc. Natl. Acad. Sci. U.S.A.* **113**, 10304–10309 (2016).
29. C. R. Shurer *et al*., Genetically encoded toolbox for glycocalyx engineering: Tunable control of cell adhesion, survival, and cancer cell behaviors. *ACS Biomater. Sci. Eng.* **4**, 388–399 (2018).
30. H. Pan, M. J. Colville, N. T. Supekar, P. Azadi, M. J. Paszek, Sequence-specific mucins for glycocalyx engineering. *ACS Synth. Biol.* **8**, 2315–2326 (2019).
31. F. Schwarz *et al*., Siglec receptors impact mammalian lifespan by modulating oxidative stress. *eLife* **4**, e06184 (2015).
32. J. Ambati, B. J. Fowler, Mechanisms of age-related macular degeneration. *Neuron* **75**, 26–39 (2012).
33. M. L. Block, L. Zecca, J. S. Hong, Microglia-mediated neurotoxicity: Uncovering the molecular mechanisms. *Nat. Rev. Neurosci.* **8**, 57–69 (2007).
34. P. J. Barnes, Alveolar macrophages as orchestrators of COPD. *COPD* **1**, 59–70 (2004).
35. H. Yu *et al*., Highly efficient chemoenzymatic synthesis of naturally occurring and non-natural α-2,6-linked sialosides: A *P. damsela* α-2,6-sialyltransferase with extremely flexible donor-substrate specificity. *Angew. Chem. Int. Ed. Engl.* **45**, 3938–3944 (2006).
36. C. S. Delaveris, E. R. Webster, S. M. Banik, S. G. Boxer, C. R. Bertozzi, Membrane-tethered mucin-like polypeptides sterically inhibit binding and slow fusion kinetics of influenza A virus. *Proc. Natl. Acad. Sci. U.S.A.* **117**, 12643–12650 (2020).
37. T. Angata, C. M. Nycholat, M. S. Macauley, Therapeutic targeting of Siglecs using antibody- and glycan-based approaches. *Trends Pharmacol. Sci.* **36**, 645–660 (2015).
38. C. D. Rillahan *et al*., On-chip synthesis and screening of a sialoside library yields a high affinity ligand for Siglec-7. *ACS Chem. Biol.* **8**, 1417–1422 (2013).
39. C. Büll *et al*., Sialic acid glycoengineering using an unnatural sialic acid for the detection of sialoglycan biosynthesis defects and on-cell synthesis of Siglec ligands. *ACS Chem. Biol.* **10**, 2353–2363 (2015).
40. H. Prescher *et al*., Synthesis and biological evaluation of 9-*N*-oxamyl sialosides as Siglec-7 ligands. *Bioorg. Med. Chem.* **23**, 5915–5921 (2015).
41. C. Büll, T. Heise, G. J. Adema, T. J. Boltje, Sialic acid mimetics to target the sialic acid-Siglec axis. *Trends Biochem. Sci.* **41**, 519–531 (2016).
42. S. Kelm, J. Gerlach, R. Brossmer, C. P. Danzer, L. Nitschke, The ligand-binding domain of CD22 is needed for inhibition of the B cell receptor signal, as demonstrated by a novel human CD22-specific inhibitor compound. *J. Exp. Med.* **195**, 1207–1213 (2002).
43. S. A. Curtin, T. J. Deming, Initiators for end-group functionalized polypeptides via tandem addition reactions. *J. Am. Chem. Soc.* **121**, 7427–7428 (1999).
44. J. Q. Zhang, G. Nicoll, C. Jones, P. R. Crocker, Siglec-9, a novel sialic acid binding member of the immunoglobulin superfamily expressed broadly on human blood leukocytes. *J. Biol. Chem.* **275**, 22121–22126 (2000).
45. E. C. Woods, N. A. Yee, J. Shen, C. R. Bertozzi, Glycocalyx engineering with a recycling glycopolymer that increases cell survival in vivo. *Angew. Chem. Int. Ed. Engl.* **54**, 15782–15788 (2015).
46. T. Angata, A. Varki, Cloning, characterization, and phylogenetic analysis of Siglec-9, a new member of the CD33-related group of Siglecs. Evidence for co-evolution with sialic acid synthesis pathways. *J. Biol. Chem.* **275**, 22127–22135 (2000).
47. A. Ishida *et al*., Negative regulation of Toll-like receptor-4 signaling through the binding of glycosylphosphatidylinositol-anchored glycoprotein, CD14, with the sialic acid-binding lectin, CD33. *J. Biol. Chem.* **289**, 25341–25350 (2014).
48. Y. Ikehara, S. K. Ikehara, J. C. Paulson, Negative regulation of T cell receptor signaling by Siglec-7 (p70/AIRM) and Siglec-9. *J. Biol. Chem.* **279**, 43117–43125 (2004).
49. S. von Gunten *et al*., Siglec-9 transduces apoptotic and nonapoptotic death signals into neutrophils depending on the proinflammatory cytokine environment. *Blood* **106**, 1423–1431 (2005).
50. M. A. Stanczak *et al*., Self-associated molecular patterns mediate cancer immune evasion by engaging Siglecs on T cells. *J. Clin. Invest.* **128**, 4912–4923 (2018).
51. T. Avril, H. Floyd, F. Lopez, E. Vivier, P. R. Crocker, The membrane-proximal immunoreceptor tyrosine-based inhibitory motif is critical for the inhibitory signaling mediated by Siglecs-7 and -9, CD33-related Siglecs expressed on human monocytes and NK cells. *J. Immunol.* **173**, 6841–6849 (2004).
52. M. Karlstetter *et al*., Polysialic acid blocks mononuclear phagocyte reactivity, inhibits complement activation, and protects from vascular damage in the retina. *EMBO Mol. Med.* **9**, 154–166 (2017).
53. I. Akhtar-Schäfer, L. Wang, T. U. Krohne, H. Xu, T. Langmann, Modulation of three key innate immune pathways for the most common retinal degenerative diseases. *EMBO Mol. Med.* **10**, 8259 (2018).
54. C. Berges *et al*., A cell line model for the differentiation of human dendritic cells. *Biochem. Biophys. Res. Commun.* **333**, 896–907 (2005).
55. M. Daigneault, J. A. Preston, H. M. Marriott, M. K. B. Whyte, D. H. Dockrell, The identification of markers of macrophage differentiation in PMA-stimulated THP-1 cells and monocyte-derived macrophages. *PLoS One* **5**, e8668 (2010).
56. M. A. Forrester *et al*., Similarities and differences in surface receptor expression by THP-1 monocytes and differentiated macrophages polarized using seven different conditioning regimens. *Cell. Immunol.* **332**, 58–76 (2018).
57. J. DiDonato *et al*., Mapping of the inducible IkappaB phosphorylation sites that signal its ubiquitination and degradation. *Mol. Cell. Biol.* **16**, 1295–1304 (1996).
58. K. Lock, J. Zhang, J. Lu, S. H. Lee, P. R. Crocker, Expression of CD33-related Siglecs on human mononuclear phagocytes, monocyte-derived dendritic cells and plasmacytoid dendritic cells. *Immunobiology* **209**, 199–207 (2004).
59. J. Davies, S. Gordon, C. Helgason, C. Miller, "Isolation and culture of human macrophages" in *Basic Cell Culture Protocols*, C. D. Helgason, C. L. Miller, Eds. (Methods in Molecular Biology, Humana Press, 2005), vol. 290, pp. 105–116.
60. S. Hong *et al*., Modulation of Siglec-7 signaling via in situ created high-affinity *cis*-ligands. bioRxiv:2020.07.15.203125 (1 September 2020).
61. N. M. Riley, J. J. Coon, Phosphoproteomics in the age of rapid and deep proteome profiling. *Anal. Chem.* **88**, 74–94 (2016).
62. M. A. Morrissey, R. D. Vale, CD47 suppresses phagocytosis by repositioning SIRPA and preventing integrin activation. bioRxiv:752311 (30 August 2019).
63. T. Kiwamoto, N. Kawasaki, J. C. Paulson, B. S. Bochner, Siglec-8 as a drugable target to treat eosinophil and mast cell-associated conditions. *Pharmacol. Ther.* **135**, 327–336 (2012).

64. S. Day *et al*., Ocular complications after anti-vascular endothelial growth factor therapy in Medicare patients with age-related macular degeneration. *Am. J. Ophthalmol.* **152**, 266–272 (2011).
65. A. Mandal *et al*., Ocular delivery of proteins and peptides: Challenges and novel formulation approaches. *Adv. Drug Deliv. Rev.* **126**, 67–95 (2018).
66. P. R. Cooper *et al*., Efflux of monoclonal antibodies from rat brain by neonatal Fc receptor, FcRn. *Brain Res.* **1534**, 13–21 (2013).
67. A. Oishi *et al*., Remission and dropout rate of anti-VEGF therapy for age-related macular degeneration. *Eur. J. Ophthalmol.* **21**, 777–782 (2011).
68. J. Kortmann, S. W. Brubaker, D. M. Monack, Cutting edge: Inflammasome activation in primary human macrophages is dependent on flagellin. *J. Immunol.* **195**, 815–819 (2015).
69. M. I. Pronobis, N. Deuitch, M. Peifer, The Miraprep: A protocol that uses a miniprep kit and provides maxiprep yields. *PLoS One* **11**, e0160509 (2016).
70. M. HaileMariam *et al*., S-trap, an ultrafast sample-preparation approach for shotgun proteomics. *J. Proteome Res.* **17**, 2917–2924 (2018).
71. S. Tyanova, T. Temu, J. Cox, The MaxQuant computational platform for mass spectrometry-based shotgun proteomics. *Nat. Protoc.* **11**, 2301–2319 (2016).
72. J. Cox *et al*., Andromeda: A peptide search engine integrated into the MaxQuant environment. *J. Proteome Res.* **10**, 1794–1805 (2011).
73. S. Tyanova *et al*., The Perseus computational platform for comprehensive analysis of (prote)omics data. *Nat. Methods* **13**, 731–740 (2016).
74. Y. Perez-Riverol *et al*., The PRIDE database and related tools and resources in 2019: Improving support for quantification data. *Nucleic Acids Res.* **47**, D442–D450 (2019).
75. C. S. Delaveris, S. H. Chiu, N. M. Riley, C. R. Bertozzi. PXD018774. ProteomeXchange. http://proteomecentral.proteomexchange.org/cgi/GetDataset?ID=PXD018774. Deposited May 5, 2019.
76. T. J. Deming, S. A. Curtin, S. Barbara, Chain initiation efficiency in cobalt- and nickel-mediated polypeptide synthesis. *J. Am. Chem. Soc.* **122**, 5710–5717 (2000).